Bo Xu, Shane Waters, Caitlin S. Byrt, Darren Plett, Stephen D. Tyerman, Mark Tester, Rana Munns, Maria Hrmova, Matthew Gilliham

Structural variations in wheat HKT1;5 underpin differences in Na+ transport capacity

Cellular and Molecular Life Sciences, 2018; 75(6):1133-1144

Full Title: Structural variations in wheat HKT1;5 underpin differences in Na^+ transport capacity

Running title: Structure-function examination of wheat HKT1;5

Authors: Bo Xu[1,2†], Shane Waters[2 †], Caitlin S. Byrt[1,2], Darren Plett[2], Stephen D. Tyerman[1,2], Mark Tester[3], Rana Munns[4], Maria Hrmova[2 *] and Matthew Gilliham[1,2*]

[1]Australian Research Council Centre of Excellence in Plant Energy Biology, University of Adelaide, Waite Research Precinct, Glen Osmond, South Australia 5064, Australia

[2]School of Agriculture, Food and Wine, and Waite Research Institute, University of Adelaide, Waite Research Precinct, Glen Osmond, South Australia 5064, Australia

[3]Center for Desert Agriculture, Division of Biological and Environmental Sciences and Engineering, 4700 King Abdullah University of Science and Technology, Thuwal 23955-6900, Kingdom of Saudi Arabia

[4]School of Agriculture and Environment, and ARC Centre of Excellence in Plant Energy Biology, University of Western Australia, Crawley 6009, Australia

[†]These authors contributed equally

[*]Corresponding authors: e-mail: matthew.gilliham@adelaide.edu.au; maria.hrmova@adelaide.edu.au

Electronic supplementary material

The online version of this article contains supplementary material

Abstract

An important trait associated with the salt tolerance of wheat is the exclusion of sodium ions (Na^+) from the shoot. We have previously shown that the sodium transporters TmHKT1;5-A and TaHKT1;5-D, from *Triticum monoccocum* (Tm) and *Triticum aestivum* (Ta), are encoded by genes underlying the major shoot Na^+-exclusion loci *Nax*1 and *Kna1*, respectively. Here, using heterologous expression we show that the affinity (K_m) for the Na^+ transport of TmHKT1;5-A, at 2.66 mM, is higher than that of TaHKT1;5-D at 7.50 mM. Through 3D structural modelling we identify residues – D^{471}/a gap and D^{474}/G^{473} that contribute to this property. We identify four additional mutations in amino acid residues that inhibit the transport activity of TmHKT1;5-A, which are predicted to be the result of an occlusion of the pore. We propose that the underlying transport properties of TmHKT1;5-A and TaHKT1;5-D contribute to their unique ability to improve Na^+ exclusion in wheat that leads to an improved salinity tolerance in the field.

Keywords: gatekeeper cells; salt exclusion; ion transport; structure-function; einkorn; bread; salt tolerance; Xenopus; mutagenesis; yeast; High affinity K^+ Transporter

Introduction

The HKT (HIGH AFFINITY (K^+) POTASSIUM TRANSPORTER) family was named when the first member of this family was identified [1]. The gene encoding this protein was cloned from a cDNA library constructed from K^+-starved wheat roots, a condition known to induce high affinity K^+-uptake in plants [1,2]. *HKT1*, now known as *TaHKT2;1*, encodes an integral membrane protein that spans the plasma membrane of the outer cell-types of *Triticum aestivum* (bread wheat) roots [1,3]. As its name suggests, and based on the protein's transport activity when observed in heterologous expression systems, TaHKT2;1 was proposed to mediate high affinity K^+ uptake in root cells [1,4]. In both *Xenopus laevis* oocytes and yeast, TaHKT2;1 functions as a K^+-Na^+ symport protein facilitating K^+ entry when external K^+ is low, by using an electrochemical gradient for Na^+ [4]. Na^+ uniport into heterologous systems and root cells has also been attributed to the TaHKT2;1 activity, when external Na^+ concentrations are in the millimolar range [1,5,6]. *TaHKT2;1* expression is also downregulated by high external Na^+ [7], through a mechanism that has been speculated to limit the entry of Na^+ into plants, which can be toxic to cells if accumulated to high levels in the cytoplasm – particularly in photosynthetic tissues [8,9].

More than twenty years after their discovery, it is now clear that HKT proteins are found widely across the plant kingdom, and, are in fact members of the high affinity K^+/Na^+ transporting Ktr/TrK/HKT superfamily of proteins present in bacteria (Ktr and TrK), fungi (TrK) and plants (HKT) [10,11]. It has recently been suggested that in bacteria, Ktr transporters could be a part of a larger protein complex that directly interact with a pump-like subunit belonging to the superfamily of P-type ATPases [12]. Based on these observations, the authors proposed a new mechanism that repurposes protein channel architecture for active transport across biomembranes.

Of the Ktr/TrK/HKT superfamily, HKT proteins are exceptional as some HKTs can facilitate Na^+ transport without co-transport of K^+. All Ktr/TrK/HKT proteins are predicted to have eight transmembrane α-helices that fold into 4-fold pseudo-tetramers around a central pore [13-15]. In plants, HKT proteins have been classified into two subfamilies; classes HKT1;*x* and HKT2;*y* [3,16], based on the transport characteristics of HKT proteins that were characterised at that stage, and using

sequences predicted to line the entry pore. The class 2 of HKT proteins has thus far only been found in monocots [15,17], and in general these proteins can facilitate K^+-Na^+ symport, or at high external concentrations Na^+-uniport. As also occurs in Ktr and TrK proteins, the selectivity filter lining the entry pore of the class 2 HKT proteins is predicted to be composed of four glycine residues; in TaHKT2;1 these are present at the protein sequence positions 91, 246, 370 and 473. In the class 1 HKT proteins the first glycine within the predicted selectivity filter is substituted with a serine residue [13]. For instance, OsHKT1;5 has a glycine present at the positions 264, 391 and 495, and one serine residue at the position 76 [14]. The majority of class 1 HKT proteins have no reported K^+ permeability and function as Na^+ uniporters only, and this has been linked to the presence of the glycine to serine substitution [3,13-15,18].

As the HKT family shares a considerable homology and their genetic variation causes a differential transport activity in plants, it is clear that subtle changes in their protein sequences can have a profound influence on transport properties [14,19-23]. Site-directed mutagenesis has been used previously to probe differences in HKT transport properties for TaHKT2;1 [24], DmHKT1 [25], SlHKT1;2 and SpHKT1;2 [26,27], TsHKT1;2 and AtHKT1 [28], making them ideal candidates for detailed structure-function examinations. Three dimensional (3D) models of two OsHKT1;5 proteins were constructed using the crystal structure of a TrkH protein from *Vibrio parahaemolyticus* VpTrKH [14,29], and this model was used to predict functional differences between two rice alleles; however, no functional validation of residues responsible for the predicted functional differences was performed [19]. Of the HKT proteins so far characterised in *X. laevis* oocytes, they catalyse Na^+ transport in a range of affinities (e.g. K_m = ~1–76 mM for HKT1;x and 0.15 –6.7 mM for HKT2;y) [30-35]. The HKT2;y subfamily members appear to possess a higher Na^+-uptake affinity than the HKT1;x subfamily; however, HKT1;x proteins are a demonstrated resource for improving salt tolerance in a range of plant species; *e.g*. AtHKT1;1 in *A. thaliana*, OsHKT1;5 from *Oryza sativa* cv. Nona Bokra, TaHKT1;5-D from *T. aestivum* and TmHKT1;5-A from *T. monococcum* [19,33,34,36-38]. However, what the structural elements are that result in the differences in transport affinity of these proteins has not yet been determined.

We have previously shown that *HKT* genes underpin two major QTL for salt tolerance in wheat; they both encode proteins that reside on the plasma membrane of cells that surround the vasculature and withdraw Na^+ from the transpiration stream preventing it from reaching the shoot where it can do damage to photosynthetic apparatus [33,34,39,40]. Hexaploid bread wheat, *T. aestivum* has three genomes; it is the D genome carrying *TaHKT1;5-D* within the *Kna1* locus that confers the Na^+-excluding ability so important to the greater salt tolerance of bread wheat [41]. An ancestral diploid wheat relative, *Triticum monococcum* (einkorn wheat), carries the homologue *TaHKT1;5-A* on the A genome. *T. monococcum* is not a progenitor to modern wheat and was the source of the *Nax2* QTL [41]. This represents an additional source of Na^+ exclusion that was shown to produce an increase in yield of 25% in saline soil when introgressed into the tetraploid durum wheat that lacks any homologues of this gene [33].

In the current work we construct new 3D models for for HKT proteins by using a more recently solved crystal structure of the KtrB K^+ transporter from *Bacillus subtilus* [14,15,42]. We then use this model to determine the impact of particular amino acid residues on the function of TmHKT1;5-A and TaHKT1;5-D. The model indicates why several mutations abolish the function of TmHKT1;5-A and predicts the residues that result in different Na^+-transport affinities between TmHKT1;5-A and TaHKT1;5-D. The impact of mutations and residue substitutions of interest were confirmed through site-directed mutagenesis and functional characterization of these HKT proteins in *X. laevis oocytes.*

Results

G490R and K118E/L339P/Y379M mutations abolished the transport properties of TmHKT1;5-A

Munns et al. [33] functionally characterised the gene product of *TmHKT1;5-A*, which was previously proposed by Byrt et al. [41] as the candidate gene underlying the shoot Na^+ exclusion QTL *Nax2*. At this time, two other *TmHKT1;5-A* variants were isolated but not reported. In one of the *TmHKT1;5-A* variants, four nucleotides differed from the *TmHKT1;5-A* sequence lodged with NCBI (DQ646332, [33]). These variations resulted in three amino acid residue changes in TmHKT1;5-$A^{K118E/L339P/Y379M}$ (Fig. S1). A single nucleotide variation was found in an additional variant, which yielded a

single amino acid residue difference in the protein sequence of TmHKT1;5-A^{G490R} (Fig. S1). These two variants were isolated from plasmid DNA in which the gene had been inserted after it had been cloned from *T. turgidum* Line 149 and had then undergone replication in *E. coli*. The *TmHKT1;5-A* sequence without mutations (DQ646339) was amplified directly from cDNA synthesised from RNA isolated from Line 149 by Polymerase Chain Reaction (PCR). The variants identified here are unlikely to be naturally occurring in wheat as they differ in sequence from the three *HKT1;5* in *T. turgidum*, which are all present on the B genome only (DQ646333, DQ646334, DQ646335); B genome members of *HKT1;5* also have very low expression [32]. Furthermore, the A genome version of *HKT1;5* is derived from a cross with *T. monococcum* – with Line 149 fixed for this allele – so it cannot be the source of three different versions of the same gene. Instead, it is likely that the Single Nucleotide Polymorphism (SNP) changes identified in these variants originated from the spontaneous mutation of *TmHKT1;5-A* in *E. coli*. Although there is no evidence to suggest that either of two variants naturally occur in wheat, these variants provided an opportunity to investigate how variation in protein sequences may alter HKT transport properties.

We were particularly interested in the properties of TmHKT1;5-A^{G490R}. Gly is a neutral residue and the Gly490 residue is highly-conserved across most plant HKT1;5-like proteins that have been characterised or identified. The exception to this is EcHKT1;1 (also known as EcHKT1) from *Eucalyptus camaldulensis* that instead has the polar amino acid residue Ser (Fig. 1a and Fig. S2) [15,43,44]; the crystallised K^+ transporter, VpTrkH has a hydrophobic Ala residue in this position [29] (Fig. S2). The residues associated with the other TmHKT1;5-A variant were not conserved: the K118 position was occupied by a variety of residues in 84% of the sequences analysed, including Glu, whilst the L339 position was substituted by hydrophobic Met, Leu, Val, Ala, Phe, Ile or hydrophilic Thr, but never by a Pro, and the Y379 position was occupied in 92% of the analysed sequences by other polar residues or by hydrophobic Pro, Leu and Val, but never Met (Table S2).

The growth of yeast transformed with either of the two *TmHKT1;5-A* variants (TmHKT1;5-A$^{K118E/L339P/Y379M}$ or TmHKT1;5-A^{G490R}) was indistinguishable from the growth of the vector-control-containing yeast on SC-Ura plates with 10 or 200 mM

Na^+ (Fig. 1b). Yeast containing *AtHKT1;1,* a positive HKT control, known to transport Na^+ and induce a growth reduction in yeast in high salt [18] grew on media containing 10 mM Na^+ but not 200 mM Na^+ (Fig. 1b). However, growth of yeast transformed with *TmHKT1;5-A* was suppressed when grown on 10 mM Na^+ (Fig. 1b) [33]. In an arginine-phosphate (AP)-based medium with low Na^+ (< 8 µM) and K^+ (< 5 µM) [45], the growth of yeast expressing *TmHKT1;5-A* was similar to that of vector control and two *TmHKT1;5-A* variants (Fig. 1c). In the AP liquid medium with 10 mM NaCl (equivalent to the amount of Na^+ in the SC-Ura agar medium) the growth of yeast containing *TmHKT1;5-A* was suppressed compared with that of the empty-vector control and the two variants.

To understand the Na^+ transport properties of TmHKT1;5-A and the two variants TmHKT1;5-$A^{K118E/L339P/Y379M}$ and TmHKT1;5-A^{G490R}, we analysed the currents associated with expressing these proteins in *X. laevis* oocytes. First, we confirmed through confocal imaging that YFP-TmHKT1;5-A chimeric proteins were localised to the plasma membrane of oocytes (Fig. 1d). Previously, we demonstrated that oocytes injected with TmHKT1;5-A-cRNA elicited significant inward currents in the presence of Na^+ [33] and here we show they accumulated 140% higher Na^+ and 40% lower K^+ than control oocytes (Fig. 1e). Oocytes injected with either variant had similar ion contents to water-injected controls (Fig. 1e), also both variant-cRNA-injected oocytes produced currents that were insignificantly different to control oocytes (water-injected), that mediated little Na^+- or K^+-dependent inward currents (Fig. 1f, g). In comparison, oocytes expressing *TmHKT1;5-A* produced a large Na^+-dependent current which was not induced by K^+ (Fig. 1f, g). Both the data from yeast and oocytes indicated that neither of the TmHKT1;5-A variants carried any significant Na^+ currents and so were likely to be rendered non-functional by their mutations.

3D structural modelling of TaHKT1;5-D and TmHKT1;5-A

We constructed 3D models to investigate whether we could determine a structural basis for the functional observations made above (Fig. 2-3 and Fig. S3). These models were based on spatial restraints that reflect a structural similarity between the plant HKT class of proteins and the KtrB K^+ transporter from *B. subtilus* [42]. At least 100 models were constructed from each alignment and assessed by the Discrete Optimized Protein Energy (DOPE) scoring function [3], PROCHECK [46] and ProSa2003 [47].

The most favourable models were constructed on the basis of AA2 alignments [48], using the MUSCLE algorithm [49]. However the first 26 amino acid residues of TaHKT1;5-D and TmHKT1;5-A were deleted from the protein sequences before running Modeller as this section had no structural counterpart in the KtrB template. A Ramachandran plot of the KtrB template (4J7C:I), TaHKT1;5-D, TmHKT1;5-A, and the G490R and K118E/L339P/Y379M variants with PROCHECK indicated that 100% (429), 99.5% (429), 99.3% (431), 98.4% (428) and 99.5% (431) residues were in the most favoured, additionally allowed and generously allowed regions, when excluding Gly and Pro residues. The overall G-factors (estimates of stereo-chemical parameters by PROCHECK) were 0.08, -0.21, -0.19, -0.14 and -0.20, and the ProSa2003 z-scores were -8.5, -6.1, -6.1, -6.2 and -6.0 for 4J7C:I, TaHKT1;5-D, TmHKT1;5-A, G490R and K118E/L339P/Y379M, respectively. DOPE analyses [50] did not reveal any substantial deviations from the global energy profiles. To assess the level of conservation of individual amino acid residues, the TaHKT1;5-D model was analysed through the ConSurf server [51,52], using 234 sequences at 35%-95% sequence identity to TaHKT1;5-D (Table S2).

The final 3D models of TaHKT1;5-D and TmHKT1;5-A (Fig. S3a and S3b) highlighted the overall architectures of both transporters with the well-defined Ser-Gly-Gly-Gly motifs (S78, G233, G353, G457) [14,15] that form the body of the selectivity filter at its narrowest point (*cf.* black arrows in Fig. S3). These motifs are consistent with these proteins being highly selective for Na^+ over K^+, as opposed to the Gly-Gly-Gly-Gly motif seen in less-selective Na^+/K^+ HKT proteins [3], or in the bacterial superfamily K^+ transporters TrkH [29] and KtrB [42].

Structural modifications in the TmHKT1;5-A variants

We used the models to investigate whether there were any obvious structural changes that may explain the lack of function of the two TmHKT1;5-A variants (Fig. 2). Compared to the wild-type protein (Fig. 2a), the change in the Van der Waals volume of TmHKT1;5-A^{G490R} (Fig. 2b) indicates that the Arg side chain formed by the G490R substitution is likely to project into the pore, resulting is less space for ions to move through the pore. For TmHKT1;5-$A^{K118E/L339P/Y379M}$, the L339P substitution locates to a loop adjoining two α-helices (Fig. 2c), and may lead to the loss of structural flexibility in this particular part of the protein. The K118E substitution is

also positioned on a loop, but is located in the proximity of two short neighbouring α-helices that may be affected by the negative charge of original Glu. This non-conservative substitution from basic Lys to acidic Glu could have a significant impact on the stability of this part of the structure. The third substitution Y379M takes place within the protein cavity that opens from the distal part of the selectivity filter, and is positioned on a short loop linking two α-helices that form the outer scaffold of the protein. While this substitution is not likely to directly affect the passage of ions through the pore, we still consider it to be significant for the integrity of the protein structure. The presence of the aromatic moiety of Tyr at the interface of two α-helices could be important for close packing and co-ordination of the dynamics of the neighbouring α-helices, and thus this Y379M substitution could destabilise this inter-α-helical interactions. We did not probe these mutations further as they make the protein non-functioinal, instead we explored whether we could use the molecular model we constructed to examine whether we could improve the transport function of the HKT proteins.

The structural basis of TaHKT1;5-D and TmHKT1;5-A Na^+ transport affinity

The TmHKT1;5-A and TaHKT1;5-D proteins share 95% positional sequence identity; they are 517 and 516 amino acid residues in length, respectively, with 27 residue differences between them (Table S1; Fig. S4). However, TmHKT1;5-A has been reported to have a lower K_m for Na^+ transport than TaHKT1;5-D [33,34]. The comparisons of the structural models for TmHKT1;5-A and TaHKT1;5-D allowed us to predict the residues that most likely contribute to structural differences between the two proteins, and therefore are likely to underlie the differences in transport affinity (Fig. 3). Six amino acid residue substitutions, which are likely to have significant structural implications have been summarized in Table 1, and are also displayed in Figs. 3 and S4. When superimposed, the respective D^{471}/a gap (or a deletion) and D^{474}/G^{473} motifs, in TmHKT1;5-A or TaHKT1;5-D were deemed as candidates likely to have the most profound impact on HKT structures and thus affect transport rates. Interestingly, the D471 position in TmHKT1;5-A was altered only in 15% sequences to mostly polar residues, such as Ser, Asp, Glu and Lys, but also to hydrophobic Ala and Pro, while the D474 position was highly variable and in 87% sequences was occupied by other 19 residues (Table S2).

D^{471}/a gap and D^{474}/G^{473} differentiate the Na^+ transport affinity of TmHKT1;5-A and TaHKT1;5-D

We further examined D^{471}/a gap and D^{474}/G^{473} using site-directed mutagenesis to explore whether these mutations affected the Na^+ transport activity of TmHKT1;5-A and TaHKT1;5-D. Initially to confirm the differential Na^+ transport activity of TmHKT1;5-A and TaHKT1;5-D [31,32] we expressed each gene in *X. laevis* oocytes and found that the Na^+ transport affinity of TmHKT1;5-A was significantly higher than of TaHKT1;5-D, by three-fold (K_m = 2.66 ± 0.35 vs. 7.5 ± 1.24 mM; *P=0.0028*, Students t-test) (Fig. 4-5). Therefore, we performed a mutagensis by PCR to delete D^{471} (TmHKT1;5-$A^{D471\Delta}$), mutate D^{474} into G (TmHKT1;5-A^{D474G}) or delete/mutate both residues (TmHKT1;5-$A^{D471\Delta/D474G}$). In addition, TaHKT1;5-D was mutated with an insertion of D^{471} (TaHKT1;5-D^{D471+}), a mutation of G^{473} into D (TaHKT1;5-D^{G473D}) and a double mutation (TaHKT1;5-$D^{D471+/G473D}$). When expressed in *X. laveis* oocytes and irrigated with a 5 mM Na^+ solution, the oocytes containing the double mutation D471Δ/D474G in TaHKT1;5-A showed a significant reduction in the Na^+ conductance from 46.19 ± 13.25 µS (of TmHKT1;5-A) to 18.22 ± 2.65 µS (of TmHKT1;5-$A^{D471\Delta/D474G}$) (Fig. 4a, b). These double mutations also led to a significant decrease in the Na^+ transport affinity of this variant from K_m = 2.66 ± 0.35 mM of wild-type TmHKT1;5-A to 4.10 ± 0.42 mM (Fig. 4a,c). The single mutation of either D471Δ or D474G increased K_m values (respective values are 3.28 ± 0.53 mM and 4.62 ± 1.29 mM), but these were statistically insignificant (Fig. 4c).

The reciprocal mutations were peformed on TaHKT1;5-D. The single mutation G473D and double mutation $D471^+$/G473D significantly increased the conductance of TaHKT1;5-D from 25.54 ± 5.78 µS to 66.2 ± 8.49 µS and 69.35 ± 9.58 µS in 5 mM Na^+ solution respectively (Fig. 5a, b). Again, only the double mutation significantly changed its transport affinity (K_m = 3.93 ± 0.57 mM), with the single mutations – $D471^+$ and G473D leading to insignificant changes in the Na^+ transport affinity of TaHKT1;5-D, to K_m = 4.48 ± 1.2 mM and 5.01 ± 0.77 mM, respectively (Fig. 5c).

Discussion

Crystal structures of the potassium ion transporters TrkH protein from *Vibrio paraheamolyticus* and KtrB from *B. subtilus* have been solved [29,42]. These

bacterial proteins together with plant HKT proteins are all part of the same superfamily of K^+ transporters [15]. However, the KtrB template has a better sequence similarity to the HKT1;5 class of proteins than that of the TrkH K^+ transporter previously used to model rice HKT1;5 proteins [14] and HKT proteins in wheat [23]. Compared to the previous model the positioning of loops connecting the α-helices and the C-terminal ends of the proteins had an improved structural similarity, although this was still only at 23% sequence identity. However, the α-helical bundle component of the TaHKT1;5-D and TmHKT1;5-A proteins aligned well with the KtrB template indicating a reliable modelling of their structure and therefore the model we propose here is an advance; a crystal structure of a HKT would obviously lend a better model, but until that occurs this is the best structural model for wheat HKT1;5 class proteins currently available. Therefore, we used this new HKT model to investigate the structural and functional differences between HKT1;5 proteins.

Our functional studies indicated that two variants TmHKT1;5-A^{G490R} and TmHKT1;5-$A^{K118E/L339P/Y379M}$, were non-functional. Despite the protein being localised in the plasma membrane, no Na^+ currents were detected when expressed in *X. laevis* oocytes and no Na^+-induced growth inhibition of *S. cerevisiae* was apparent unlike in yeast expressing *TmHKT1;5-A* (Fig. 1). In Fig. 1a and Fig. S2, it can be seen that the Gly490 residue is highly conserved in other HKT1;5-A-like proteins, suggesting that it is an important residue for transport function or for structural integrity. Our structural analysis indicated that the TmHKT1;5-A^{G490R} substitution occurred in a side chain that carries a positive charge at physiological pH. This combined with its likely steric hindrance obstructing the pore, would present a barrier to cations moving through the extension of the selectivity filter (Fig. 2 and Fig. S3). Furthermore, this mutation may affect the pore rigidity and dispositions of neighbouring residues controlling the rates of Na^+ transport. Therefore, in summary, the structural penalties caused by the G490R variation may work in concert and explain the loss of Na^+ transport activity by this variant of the TmHKT1;5-A protein. For, TmHKT1;5-$A^{K118E/L339P/Y379M}$, all the amino acid residue substitutions are non-conservative (Table S2). Y379 was found to be the least conserved of the three, this position was usually occupied by an aromatic residue with Ser being a common exception. The K118E and Y379M substitutions were only observed in 1% of the

sequences, while the L339P substitution remained undetected. As described in the results, we propose that these three substitutions largely destabilise the TmHKT1;5-A structure and result in a loss of function.

Using our molecular models, we turned our attention to making predictions regarding the residue differences that are likely to contribute to the higher affinity of Na^+ transport observed for TmHKT1;5-A compared to TaHKT1;5-D (Fig. 4 and 5). There are 27 amino acid residue differences between these two proteins, and through our analysis we predicted that six residue substitutions were likely to be significant (Table 1 and Fig. 3). Of these six, there were two residues, D471 and D474 from TmHKT1;5-A that were particularly interesting because this combined pair of aspartic acids at these sites were not observed in any of 48 other HKT members analysed, except OsHKT2;4 which has an aspartic acid at the site 466 but an alanine at site 469 (Fig. S5). Indeed, the D471/a gap and D474/473G substitutions occur very close to each other and form a part of an α-helix which directly links to one of the loops forming the selectivity filter. Double mutations of these two residues – D471Δ/D473G and D471$^+$/G473D, respectively, – caused a reduction in the TmHKT1;5-A Na^+ transport affinity while increasing it for TaHKT1;5-D. This resulted in the Na^+ transport affinity of TmHKT1;5-A$^{D471\Delta/D474G}$ (K_m = ~3.9 mM) and TaHKT1;5-D$^{D471+/G473D}$ (K_m = 4.1 mM) to be at a similar level. Nevertheless, TmHKT1;5-A$^{D471\Delta/D474G}$ still had a higher Na^+ transport affinity than wild-type TaHKT1;5-D (P = 0.0076), suggesting that other substitutions listed in Table S1 are likely to further contribute to the observed functional differences. The D471Δ/D473G substitutions decreased the transport conductance of TmHKT1;5-A$^{D471\Delta/D474G}$, close to that of TaHKT1;5-D (P = 0.6439); while TaHKT1;5-D$^{D471+/G473D}$ had a comparable conductance to TmHKT1;5-A (P = 0.5136) (Fig. 4a, b). So these two motifs (D471/a gap and G473/474D) have a key influence on the Na^+-uptake capacity of TmHKT1;5-A/TaHKT1;5-D. We did not find evidence that these mutations are naturally occurring within wheat, but these could be investigated in the future through the use of molecular markers on wheat diversity panels. An extension of the model to include other HKT proteins, a greater survey of structure-function relationships and experimental mutations of key residues both in *vitro* and *in vivo* to explore the wider functional significance of these differences will be the focus of a further study.

TmHKT1;5-A facilitates Na^+ uptake with a higher affinity than TaHKT1;5-D (Fig. 4-5). We studied the K_m of these proteins, as this is the parameter in which we could have most confidence. Whereas V_{max} may be susceptible to misinterpretation due to potential differences in protein expression between *X. laevis* oocytes, K_m values will not. Importantly, physiologically relevant concentrations in the stele (i.e. in the low mM range; Table III [8]), coincide with the K_m of TmHKT1;5-A. This suggests that the higher mM values for the K_m of TaHKT1;5-D would render it less effective in retrieving Na^+ into stelar cells and therefore is a potential explanation of how it confers less Na^+ exclusion. Consistent with this proposition, the introgression of the *Nax2* locus carrying *TmHKT1*;5-A into bread wheat confers greater Na^+-exclusion to bread wheat which already carries *TaHKT1*;5-D [53].

The expression of class 1 *HKT* genes can elicit downstream responses that lead to an increased exclusion of Na^+ from the shoot [33,34,37,38]. We envisage that HKT1;5-like proteins may stimulate retrieval of Na^+ from the stelar apoplast, specifically from the xylem vessel elements, and effectively act as a node setting off a cascade of downstream processes that lead to greater plant salt tolerance. These processes involve the increased activity of proteins involved in compartmentation of Na^+ within the root vacuoles of specific cell-types and the cortex [9,37,38] and potentially those that catalyse the efflux of Na^+ from roots. Stelar cells, and in particular those cells that line the xylem, clearly play an important role in limiting the salt transport to the shoot and in conferring plant salt tolerance. As such, we consider it instructive to think of this action as constituting a 'gatekeeper' process. *i.e.* a discrete cell-type that provides a rate limiting step for the control the flux of solutes into or throughout the plant, be they nutrients, toxins or metabolites. We consider that it is imperative that the unique transport processes within populations of these gatekeeper cell-types are further studied to understand how the net flux of solutes through plant tissues occurs [54].

Coupling previous research [33,34] with the comparison of two Na^+-selective channels in this study suggests that the candidate gene *TmHKT1*;5-*A* in the *Nax2* locus from ancestral wheat germplasm *T. monococcum* encodes a unique high affinity Na^+-exclusion transporter. We propose that this locus serves as an optimal choice for wheat breeders for developing salinity tolerant wheat lines with more efficient Na^+-exclusion.

Materials and Methods

Brief methods for cloning of *TmHKT1;5-A* and variants as well as its functional characterisation in heterologous expression systems of *X. laevis* oocyte and *Saccharomyces cerevisiae* were described Munns et al. [33] and Byrt et al. [34]. More detailed methods for protein modelling were included in Cotsaftis et al. [14]. Further details are included here.

Gene cloning and site-directed mutagenesis

TmHKT1;5-A was isolated from both cDNA of durum wheat (*T. turgidum*) Line 149 roots and the *T. monococcum* (DV92) BAC library [33,34,41,55]. The following site-directed-mediated mutagenesis PCR was performed on these entry clones as templates to create single or double mutations of *TmHKT1;5-A* and *TaHKT1;5-D* as indicated in a Figure legend, using the Phusion™ Hot Start High-Fidelity DNA polymerase (FINNZYMES) with primers as listed in Table S3. PCR products were purified from agarose gel sand phosphorylated by the T4 Polynucleotide Kinase (New England Biolabs) to add a phosphate group to the 5' and 3' ends of the products at 37 ºC for 30 min. These were subsequently self-ligated by the T4 DNA Ligase (New England Biolabs) at 4 ºC overnight. Ligase reactions were transformed into TOP10 Chemically Competent *E. coli* cells (Invitrogen).

Plasmid contruction

The vector containing a YFP tag for heterologous expression in *X. laevis* oocytes was constructed using a restriction digest and ligation of two expression vector fragments. The pGEMHE-DEST vector for *X. laevis* oocyte expression was cut by *Sma*I and *Xba*I to remove the Gateway cloning site and to provide a backbone; then the same enzyme set was used to cut the Gateway cloning cassette with *YFP* tagged on the N-terminus from pBS-YFP-attR. Two fragments were fused together into a new expression vector named pYFP-GEMHE using the T4 ligase (New England Biolabs). *TmHKT1;5-A*$^{K118E/L339P/Y379M}$ and *TmHKT1;5-A*^{G490R} were recombined from the entry vector into the new pYFP-GEMHE using Gateway LR Clonase II Enzyme mix (Invitrogen).

Fluorescence imaging of TmHKT1;5-A variant to investigate membrane localisation in *X. laevis* oocytes

The recombinant expression vector pYFP-GEMHE carrying *TmHKT1;5-A*$^{K118E/L339P/Y379M}$ or *TmHKT1;5-A*^{G490R} was linearised by *Sbf*I (New England Biolabs). cRNA was synthesised from linearised plasmid using the mMESSAGE mMACHINE T7 Transcription Kit, following manufacturer's instructions (Ambion). 46 nl/46 ng of cRNA was injected into oocytes with a Nanoinject II microinjector (Drummond Scientific). Oocytes were incubated for 48 h at 18 ºC before imaging using a confocal laser scanning microscope equipped with a Zeiss Axioskop 2, LSM5 PASCAL and an argon laser (Carl Zeiss). Sequential scanning and laser excitation was used to capture fluorescence from YFP (excitation = 514 nm, emission band pass = 570–590 nm).

Two-electrode voltage clamp recording in *X. laevis* oocytes

Oocyte recording followed the methods as described in Munns et al. [33] and Byrt et al. [34]. Briefly, 46 nl/23 ng of cRNA or equal volumes of RNA-free water were injected into oocytes, followed by an incubation for 48 h before recording. Membrane currents were recorded in the HMg solution (6 mM $MgCl_2$, 1.8 mM $CaCl_2$, 10 mM MES and pH 6.5 adjusted with a TRIS base) ± Na^+ glutamate and/or K^+ glutamate as indicated. All solution osmolarities were adjusted using mannitol at 220-240 mOsmol kg^{-1}.

Construction of 3D models of TaHKT1;5-D, TmHKT1;5-A and the G490R and K118E/L339P/Y379M variants of TmHKT1;5-A

The most suitable template for TaHKT1;5-D, TmHKT1;5-A and variants of TmHKT1;5-A, identified by Phyre2 [56] and I-TASSER [57], was the KtrB K^+ transporter from *B. subtilis* (Protein Data Bank accession 4J7C, chain I referred to as 4J7C:I) [42]. This template replaces the TrkH K^+ transporter (Protein Data Bank accession 3PJZ, chain K referred to as 3PJZ:K) [29] that was previously used to model rice HKT proteins [14]. The KtrB K^+ structure was crystallised in the presence of 150 mM KCl and contains a K^+ ion in the central pore. This ion was substituted by Na^+ ion during modelling of wheat HKT proteins because TaHKT1;5-D and TmHKT1;5-A proteins transport Na^+ and not K^+. As the respective sequence identity and similarity between TmHKT1;5-A and 4J7C:I (23% and 59%), and TaHKT1;5-D and 4J7C:I (23% and 61%) were low a variety of alignments obtained through

LOMETS [58], PROMALS3D [59], MUSCLE [49] and AA2 [48] were applied to generate models in complex with Na^+, using Modeller 9v8 [60] on a Linux station running the Fedora 12 operating system.

Statistical analysis

All analysis and graphing was performed in Graphpad Prism version 7. Statistical tests were performed as stated in the text or figure legends.

Funding

This work was supported by the Grains Research and Development Corporation (UA00145, M.G.), the University of Adelaide Australian Postgraduate Award and the CJ Everald postgraduate scholarship (S.W.), and the Australian Research Council through the following schemes: Discovery (DP120100900, M.H.), Centre of Excellence (CE140100008, M.G., R.M., S.D.T), Future Fellowship (FT130100709, M.G.), and DECRA (DE150100837, C.S.B.).

Author contribution

B.X., M.H., D.P. and M.G. conceived the project out of work initiated by R.M. and M.T.. B.X. performed all experiments except the structural modelling and predictions (S.W.) and the cloning and original characterisation of TmHKT1;5-$A^{K118E/L339P/Y379M}$ (C.S.B.). S.D.T. advised on electrophysiology and analysis. M.G, M.H. and D.P. supervised the work. B.X., S.W., C.S.B., M.H. and M.G. wrote the paper. All authors provided comment.

Acknowledgements

N/A

References

1. Schachtman DP, Schroeder JI (1994) Structure and transport mechanism of a high-affinity potassium uptake transporter from higher plants. Nature 370:655-658
2. Epstein E (1966) Dual pattern of ion absorption by plant cells and by plants. Nature 212:1324-1327
3. Platten JD, Cotsaftis O, Berthomieu P, Bohnert H, Davenport RJ, Fairbairn DJ, Horie T, Leigh RA, Lin H-X, Luan S (2006) Nomenclature for HKT transporters, key determinants of plant salinity tolerance. Trends Plant Sci 11 (8):372-374

4. Rubio F, Gassmann W, Schroeder JI (1995) Sodium-driven potassium uptake by the plant potassium transporter HKT1 and mutations conferring salt tolerance. Science 270 (5242):1660-1663
5. Gierth M, Mäser P (2007) Potassium transporters in plants–involvement in K^+ acquisition, redistribution and homeostasis. FEBS Lett 581 (12):2348-2356
6. Horie T, Hauser F, Schroeder JI (2009) HKT transporter-mediated salinity resistance mechanisms in *Arabidopsis* and monocot crop plants. Trends Plant Sci 14 (12):660-668
7. Laurie S, Feeney KA, Maathuis FJ, Heard PJ, Brown SJ, Leigh RA (2002) A role for HKT1 in sodium uptake by wheat roots. Plant J 32 (2):139-149
8. James RA, Davenport RJ, Munns R (2006) Physiological characterization of two genes for Na^+ exclusion in durum wheat, *Nax1* and *Nax2*. Plant Physiol 142 (4):1537-1547
9. Läuchli A, James RA, Huang CX, McClluy M, Munns R (2008) Cell-specific localization of Na^+ in roots of durum wheat and possible control points for salt exclusion. Plant Cell Environ 31 (11):1565-1574
10. Sentenac H, Bonneaud N (1992) Cloning and expression in yeast of a plant potassium ion transport system. Science 256 (5057):663-665
11. Corratgé-Faillie C, Jabnoune M, Zimmermann S, Véry A-A, Fizames C, Sentenac H (2010) Potassium and sodium transport in non-animal cells: the Trk/Ktr/HKT transporter family. Cell Mol Life Sci 67 (15):2511-2532
12. Huang CS, Pedersen BP, Stokes DL (2017) Crystal structure of the potassium-importing KdpFABC membrane complex. Nature 546 (7660):681-685
13. Mäser P, Hosoo Y, Goshima S, Horie T, Eckelman B, Yamada K, Yoshida K, Bakker EP, Shinmyo A, Oiki S (2002) Glycine residues in potassium channel-like selectivity filters determine potassium selectivity in four-loop-per-subunit HKT transporters from plants. Proc Natl Acad Sci USA 99 (9):6428-6433
14. Cotsaftis O, Plett D, Shirley N, Tester M, Hrmova M (2012) A two-staged model of Na^+ exclusion in rice explained by 3D modeling of HKT transporters and alternative splicing. PLoS One 7 (7):e39865
15. Waters S, Gilliham M, Hrmova M (2013) Plant high-affinity potassium (HKT) transporters involved in salinity tolerance: structural insights to probe differences in ion selectivity. Int J Mol Sci 14 (4):7660-7680
16. Singh A, Bhushan B, Gaikwad K, Yadav OP, Kumar S, Rai RD (2015) Induced defence responses of contrasting bread wheat genotypes under differential salt stress imposition. Indian J Biochem Biophys 52 (1):75-85
17. Asins MJ, Villalta I, Aly MM, Olias R, Álvarez De Morales P, Huertas R, Li J, Jaime-Pérez N, Haro R, Raga V (2013) Two closely linked tomato HKT coding genes are positional candidates for the major tomato QTL involved in Na^+/K^+ homeostasis. Plant Cell Environ 36 (6):1171-1191
18. Uozumi N, Kim EJ, Rubio F, Yamaguchi T, Muto S, Tsuboi A, Bakker EP, Nakamura T, Schroeder JI (2000) The Arabidopsis HKT1 gene homolog mediates inward Na^+ currents in *Xenopus laevis* oocytes and Na^+ uptake in *Saccharomyces cerevisiae*. Plant Physiol 122 (4):1249-1260
19. Ren ZH, Gao JP, Li LG, Cai XL, Huang W, Chao DY, Zhu MZ, Wang ZY, Luan S, Lin HX (2005) A rice quantitative trait locus for salt tolerance encodes a sodium transporter. Nat Genet 37 (10):1141-1146
20. Negrão S, Cecília Almadanim M, Pires IS, Abreu IA, Maroco J, Courtois B, Gregorio GB, McNally KL, Margarida Oliveira M (2013) New allelic variants

found in key rice salt-tolerance genes: an association study. Plant Biotech J 11 (1):87-100
21. Ariyarathna HCK, Ul-Haq T, Colmer TD, Francki MG (2014) Characterization of the multigene family TaHKT 2;1 in bread wheat and the role of gene members in plant Na^+ and K^+ status. BMC Plant Biol 14 (1):1
22. Mishra S, Singh B, Panda K, Singh BP, Singh N, Misra P, Rai V, Singh NK (2016) Association of SNP haplotypes of HKT family genes with salt tolerance in indian wild rice germplasm. Rice 9 (1):1
23. Kumar S, Beena A, Awana M, Singh A (2017) Physiological, biochemical, epigenetic and molecular analyses of wheat (*Triticum aestivum*) genotypes with contrasting salt tolerance. Front Plant Sci 8:1151
24. Diatloff E, Kumar R, Schachtman DP (1998) Site directed mutagenesis reduces the Na^+ affinity of HKT1, an Na^+ energized high affinity K^+ transporter. FEBS Lett 432 (1-2):31-36
25. Böhm J, Scherzer S, Shabala S, Krol E, Neher E, Mueller T, Hedrich R (2016) *Venus flytrap* HKT1-type channel provides for prey sodium uptake into carnivorous plant without conflicting with electrical excitability. Mol Plant 9 (3):428-436
26. Almeida P, Katschnig D, de Boer AH (2013) HKT transporters-state of the art. Int J Mol Sci 14 (10):20359-20385
27. Almeida P, de Boer G-J, de Boer AH (2014) Differences in shoot Na^+ accumulation between two tomato species are due to differences in ion affinity of HKT1;2. J Plant Physiol 171 (6):438-447
28. Ali A, Raddatz N, Aman R, Kim S, Park HC, Jan M, Baek D, Khan IU, Oh D-H, Lee SY (2016) A single amino acid substitution in the sodium transporter HKT1 associated with plant salt tolerance. Plant Physiol 171: 2112–2126
29. Cao Y, Jin X, Huang H, Derebe MG, Levin EJ, Kabaleeswaran V, Pan Y, Punta M, Love J, Weng J (2011) Crystal structure of a potassium ion transporter, TrkH. Nature 471 (7338):336-340
30. Mian A, Oomen RJ, Isayenkov S, Sentenac H, Maathuis FJ, Véry AA (2011) Over-expression of an Na^+-and K^+-permeable HKT transporter in barley improves salt tolerance. Plant J 68 (3):468-479
31. Jabnoune M, Espeout S, Mieulet D, Fizames C, Verdeil J-L, Conéjéro G, Rodríguez-Navarro A, Sentenac H, Guiderdoni E, Abdelly C (2009) Diversity in expression patterns and functional properties in the rice HKT transporter family. Plant Physiol 150 (4):1955-1971
32. Amar SB, Brini F, Sentenac H, Masmoudi K, Véry A-A (2014) Functional characterization in *Xenopus* oocytes of Na^+ transport systems from durum wheat reveals diversity among two HKT1;4 transporters. J Exp Bot 65 (1):213-222
33. Munns R, James RA, Xu B, Athman A, Conn SJ, Jordans C, Byrt CS, Hare RA, Tyerman SD, Tester M, Plett D, Gilliham M (2012) Wheat grain yield on saline soils is improved by an ancestral Na^+ transporter gene. Nat Biotech 30 (4):360-364
34. Byrt CS, Xu B, Krishnan M, Lightfoot DJ, Athman A, Jacobs AK, Watson-Haigh NS, Plett D, Munns R, Tester M (2014) The Na^+ transporter, TaHKT1;5-D, limits shoot Na^+ accumulation in bread wheat. Plant J 80 (3):516-526
35. Tounsi S, Amar SB, Masmoudi K, Sentenac H, Brini F, Véry A-A (2016) Characterization of two HKT1;4 transporters from *Triticum monococcum* to elucidate the determinants of the wheat salt tolerance *Nax1* QTL. Plant Cell Physiol 57 (10):2047-2057

36. Baxter I, Brazelton JN, Yu D, Huang YS, Lahner B, Yakubova E, Li Y, Bergelson J, Borevitz JO, Nordborg M (2010) A coastal cline in sodium accumulation in *Arabidopsis thaliana* is driven by natural variation of the sodium transporter AtHKT1; 1. PLoS Genet 6 (11):e1001193
37. Møller IS, Gilliham M, Jha D, Mayo GM, Roy SJ, Coates JC, Haseloff J, Tester M (2009) Shoot Na^+ exclusion and increased salinity tolerance engineered by cell type-specific alteration of Na^+ transport in Arabidopsis. Plant Cell 21 (7):2163-2178
38. Plett D, Safwat G, Gilliham M, Møller IS, Roy S, Shirley N, Jacobs A, Johnson A, Tester M (2010) Improved salinity tolerance of rice through cell type-specific expression of *AtHKT1; 1*. PLoS One 5 (9):e12571
39. Munns R, Gilliham M (2015) Salinity tolerance of crops–what is the cost? New Phytol 208 (3):668-673
40. Ismail AM, Horie T (2017) Genomics, physiology, and molecular breeding approaches for improving salt tolerance. Annu Rev Plant Biol 68:405-434
41. Byrt CS, Platten JD, Spielmeyer W, James RA, Lagudah ES, Dennis ES, Tester M, Munns R (2007) HKT1; 5-like cation transporters linked to Na^+ exclusion loci in wheat, *Nax2* and *Kna1*. Plant Physiol 143 (4):1918-1928
42. Vieira-Pires RS, Szollosi A, Morais-Cabral JH (2013) The structure of the KtrAB potassium transporter. Nature 496 (7445):323-328
43. Fairbairn DJ, Liu W, Schachtman DP, Gomez-Gallego S, Day SR, Teasdale RD (2000) Characterisation of two distinct HKT1-like potassium transporters from *Eucalyptus camaldulensis*. Plant Mol Biol 43 (4):515-525
44. Liu W, Fairbairn DJ, Reid RJ, Schachtman DP (2001) Characterization of two HKT1 homologues from *Eucalyptus camaldulensis* that display intrinsic osmosensing capability. Plant Physiol 127 (1):283-294
45. Rodríguez-Navarro A, Ramos J (1984) Dual system for potassium transport in *Saccharomyces cerevisiae*. J Bacteriol 159 (3):940-945
46. Laskowski RA, MacArthur MW, Moss DS, Thornton JM (1993) PROCHECK: a program to check the stereochemical quality of protein structures. J Appl Crystallogr 26 (2):283-291
47. Sippl MJ (1993) Recognition of errors in three-dimensional structures of proteins. Proteins 17 (4):355-362
48. Gille C, Birgit W, Gille A (2013) Sequence alignment visualization in HTML5 without Java. Bioinformatics 30 (1):121-122
49. Edgar RC (2004) MUSCLE: multiple sequence alignment with high accuracy and high throughput. Nucleic Acids Res 32 (5):1792-1797
50. Shen My, Sali A (2006) Statistical potential for assessment and prediction of protein structures. Protein Sci 15 (11):2507-2524
51. Landau M, Mayrose I, Rosenberg Y, Glaser F, Martz E, Pupko T, Ben-Tal N (2005) ConSurf 2005: the projection of evolutionary conservation scores of residues on protein structures. Nucleic Acids Res 33 (suppl 2):W299-W302
52. Celniker G, Nimrod G, Ashkenazy H, Glaser F, Martz E, Mayrose I, Pupko T, Ben-Tal N (2013) ConSurf: using evolutionary data to raise testable hypotheses about protein function. Isr J Chem 53 (3-4):199-206
53. James RA, Blake C, Byrt CS, Munns R (2011) Major genes for Na^+ exclusion, *Nax1* and *Nax2* (wheat *HKT1;4* and *HKT1;5*), decrease Na^+ accumulation in bread wheat leaves under saline and waterlogged conditions. J Exp Bot 62 (8):2939-2947

54. Henderson SW, Gilliham M (2015) The “Gatekeeper” Concept: Cell-Type Specific Molecular Mechanisms of Plant Adaptation to Abiotic Stress. In: Molecular Mechanisms in Plant Adaptation. pp 83-115
55. Byrt CS (2008) PhD thesis: Genes for sodium exclusion in wheat. University of Adelaide,
56. Kelley LA, Sternberg MJ (2009) Protein structure prediction on the Web: a case study using the Phyre server. Nat Protoc 4 (3):363-371
57. Zhang Y (2008) I-TASSER server for protein 3D structure prediction. BMC Bioinformatics 9 (1):1
58. Wu S, Zhang Y (2007) LOMETS: a local meta-threading-server for protein structure prediction. Nucleic Acids Res 35 (10):3375-3382
59. Pei J, Kim BH, Grishin NV (2008) PROMALS3D: a tool for multiple protein sequence and structure alignments. Nucleic Acids Res 36 (7):2295-2300
60. Sali A, Blundell T (1993) Comparative protein modelling by satisfaction of spatial restraints. J Mol Biol 234 (3):779-815

FIGURES AND FIGURE LEGENDS

Fig. 1 Mutation of G490R and K118E/L339P/Y379M in TmHKT1;5-A inhibited its Na^+ transport in heterologous expression systems. **a.** Protein sequence alignment of *HKT1;5* homologues from wheat, rice, barley, sorghum, *Medicago truncatula* and Arabidopsis. The blue box indicates the 490 residue position of TmHKT1;5-A and its homologues. The protein accession number are TmHKT1;5-A, ABG33946.1; TaHKT1;5-B1, ABG33947.1; TaHKT1;5-B2, ABG33948.1; TaHKT1;5-D, ABG33949.1; TtHKT1;5-B1, ABG33940.1; TtHKT1;5-B2, ABG33941.1; HvHKT1;5, ABK58096.1;.OsHKT1;5-Ni, Q0JNB6.1; OsHKT1;5-Po, A2WNZ9.2; AtHKT1;1, Q84TI7.1; SbiHKT1;5, EES02856.1; MtHKT1;5, AES77170.1; Tm, *Triticum monococcum*; Ta, *Triticum aestivum*; Tt, *Triticum turgidum* subsp. *durum*; Hv, *Hordeum vulgare*; Os, *Oryza sativa*; At, *Arabidopsis thaliana*; Sbi, *Sorghum bicolor*; Mt, *Medicago truncatula*. **b, c** Growth of *S. cerevisiae* strain InvSc2 (MATa his-D1 leu2 trp1-289 ura3-52) expressing *TmHKT1;5-A*, its two variants and empty-vector control on either the SC-Ura agar medium (**b**) or the AP liquid medium (**c**). **b** A five serial dilutions of yeasts were spotted on the SC-Ura medium with 2% (w/v) Gal, 1.67% (w/v) agar and indicated Na level present and incubated at 30 ºC for three days. **c** Optical density at 600 nm of yeast growth in the liquid AP medium containing 0 mM or 10 mM NaCl. Data represented in mean ± S.E.M, n = 3. **d-g** Heterologous expression of TmHKT1;5-A and its two variants in *X. laevis* oocytes. **d** Confocal images of oocytes expressing two variants tagged with *YFP* at the N-terminus. **e** Relative change in the ion profile of oocytes expressing *TmHKT1;5-A* and its two variants to uninjected oocytes, data represented in mean ± S.E.M, n = 3. **f** and **g** Current-voltage (I/V) curve of *X. laevis* oocytes expressing *TmHKT1;5-A*, *TmHKT1;5-A*$^{K118E/L339P/Y379M}$, *TmHKT1;5-A*^{G490R} and the H_2O-injected control. Ooytes expressing *TmHKT1;5-A* were recorded in 30 mM Na (**f**) and 10 mM K (**g**) glutamate; data represented in mean ± S.E.M, n = 5-9.

Fig. 2 Molecular models of TmHKT1;5-A and G490R and K118E/L339P/Y379M variants. Cartoon representations of wild-type TmHKT1;5-A (**a**; cyan) and the G490R (**b**; pink) and K118E/L339P/Y379M (**c**; orange) variants illustrate overall folds in two orthogonal orientations (left and right panels). The left and right views in

panels **a-c** are related by 90° rotation about the horizontal axis. The structures of 3D models are depicted in cartoon representations with cylindrical α-helices in wild-type (**a**, G490 with the Van der Waals surface) or mutant (**b**, G490R with Van der Waals surface; C, K118E, L339P, Y379M in atomic sticks) structures. Na^+ ions are shown as purple spheres located within the boundary of selectivity filters, where α-backbones of pore-forming residues are coloured in red. Four substituted residues between wild-type (**a**), and the G490R (**b**) and K118E/L339P/Y379M (**c**) variants are shown in sticks and atomic colours. **d** A stereo view of four substitutions (G490R and K118E/L339P/Y379M) shown on the opaque background of the cartoon structures with Van der Waals surfaces in colours that are identical to those shown in panels (**a-c**). Entries into the funnel of superposed transporters are indicated by a black arrows.

Fig. 3 A stereo view of superposed TmHKT1;5-A and TaHKT1;5-D. Six differences in residues that are likely to underlie functional differences between the proteins are depicted on the opaque background of cartoon structures with Van der Waals surfaces. These residues are labelled by TmHKT1;5-A (first residue) TaHKT1;5-D (last residue) numbering. The entries into the funnels of transporters are indicated by black arrows.

Fig. 4 Transport characteristics of TmHKT1;5-A, TmHKT1;5-A-D471Δ, -D474G and - D471Δ/D474G in *X. laevis* oocytes. a, b The I/V curve (**a**) and transport conductance at -140 mV (**b**) of oocytes expressing *TmHKT1;5-A*, $TmHKT1;5\text{-}A^{D471\Delta}$, $TmHKT1;5\text{-}A^{D474G}$ and $TmHKT1;5\text{-}A^{D471\Delta/D474G}$ in 5 mM Na^+ solution. **c** Na^+-transport affinity of TmHKT1;5-A, TmHKT1;5-A-D471Δ, -D474G and - D471Δ/D474G in *X. laevis* oocytes. Michaelis-Menten kinetics of relative inward current at -140 mV, of oocytes expressing *TmHKT1;5-A*, $TmHKT1;5\text{-}A^{D471\Delta}$, $TmHKT1;5\text{-}A^{D474G}$ and $TmHKT1;5\text{-}A^{D471\Delta/D474G}$ in a serial Na^+ solution of 0.01, 0.02, 0.05, 0.1, 0.5, 1, 2, 5, 10 and 30 mM. Data represent Mean ± S.E.M, n = 6-9. Statistical difference was determined by *Student's t*-test, asterick indicates statistical difference, $*P < 0.05$.

Fig. 5 Transport characteristics of TaHKT1;5-D, TaHKT1;5-D-D471$^+$, -G473D and -D471$^+$/G473D in *X. laevis* oocytes. a, b The I/V curve (**a**) and transport conductance at -140 mV (**b**) of oocytes expressing *TaHKT1;5-D*, $TaHKT1;5\text{-}D^{D471+}$, $TaHKT1;5\text{-}D^{G473D}$ and $TaHKT1;5\text{-}D^{D471+/G473D}$ in 5 mM Na^+ solution. **c** Na^+-transport

affinity of TaHKT1;5-D, TaHKT1;5-D-D471^{+}, -G473D and -D471^{+}/G473D in *X. laevis* oocytes. Michaelis-Menten kinetics of relative inward current at -140 mV, of oocytes expressing *TaHKT1;5-D*, *TaHKT1;5-D*$^{D471+}$, *TaHKT1;5-D*^{G473D} and *TaHKT1;5-D*$^{D471+/G473D}$ in a serial Na^{+} solution of 0.01, 0.02, 0.05, 0.1, 0.5, 1, 2, 5, 10 and 30 mM. Data represent Mean ± S.E.M, n = 5-6. Statistical difference was determined by *Student's t*-test, astericks indicate statistical difference, $*P < 0.05$ and $**P < 0.01$.

Table 1. A summary of differences in amino acid residues between TmHKT1;5-A and TaHKT1;5-D that are likely significantly affect transport rates.

Fig. 1

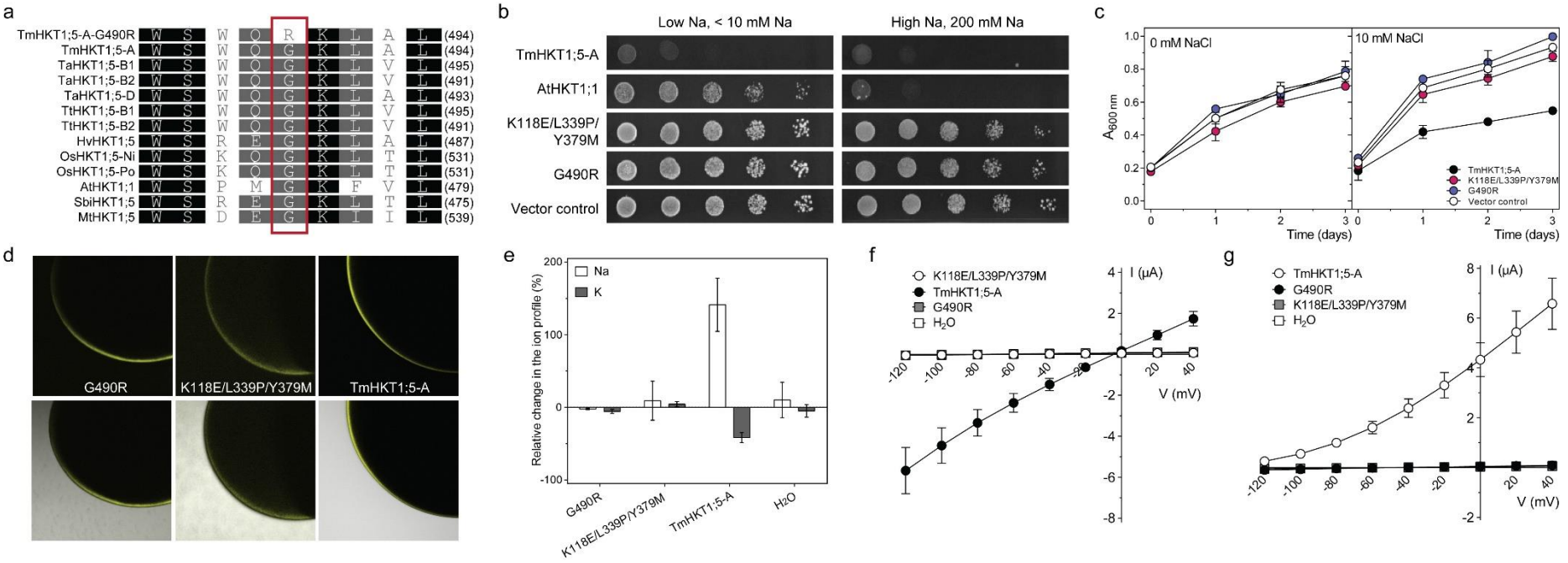
a
TmHKT1;5-A-G490R
TmHKT1;5-A
TaHKT1;5-B1
TaHKT1;5-B2
TaHKT1;5-D
TtHKT1;5-B1
TtHKT1;5-B2
HvHKT1;5
OsHKT1;5-Ni
OsHKT1;5-Po
AtHKT1;1
SbiHKT1;5
MtHKT1;5
(494)
(494)
(495)
(491)
(493)
(495)
(491)
(487)
(531)
(531)
(479)
(475)
(539)
b
Low Na, < 10 mM Na
High Na, 200 mM Na
TmHKT1;5-A
AtHKT1;1
K118E/L339P/ Y379M
G490R
Vector control
c
0 mM NaCl
10 mM NaCl
A600 nm
Time (days)
TmHKT1;5-A
K118E/L339P/Y379M
G490R
Vector control
d
G490R
K118E/L339P/Y379M
TmHKT1;5-A
e
Na
K
Relative change in the ion profile (%)
G490R
K118E/L339P/Y379M
TmHKT1;5-A
H2O
f
K118E/L339P/Y379M
TmHKT1;5-A
G490R
H2O
I (μA)
V (mV)
g
TmHKT1;5-A
G490R
K118E/L339P/Y379M
H2O
I (μA)
V (mV)

Fig. 2

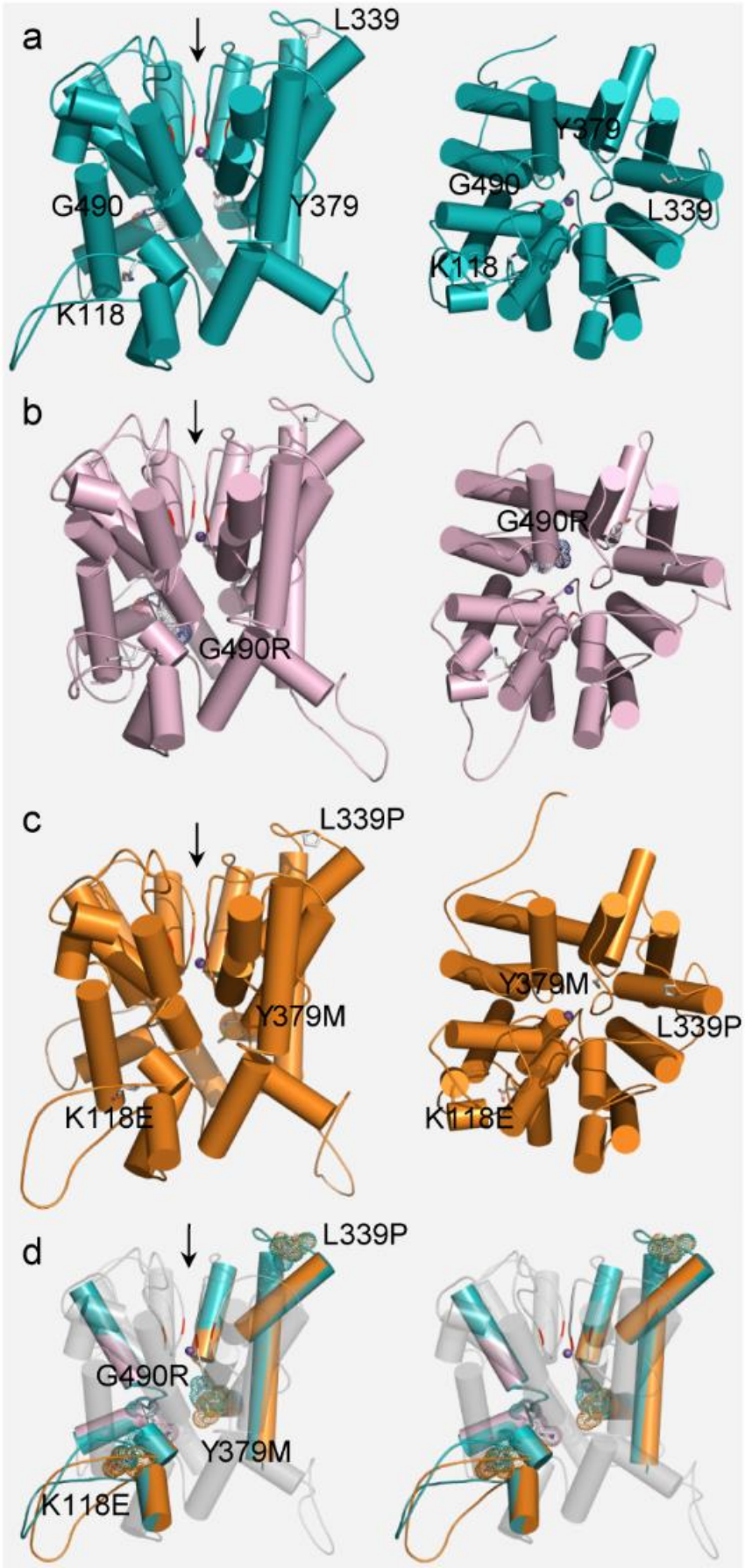
a
L339
G490
Y379
K118
Y379
G490
L339
K118
b
G490R
G490R
c
L339P
Y379M
K118E
Y379M
L339P
K118E
d
L339P
G490R
Y379M
K118E

Fig. 3

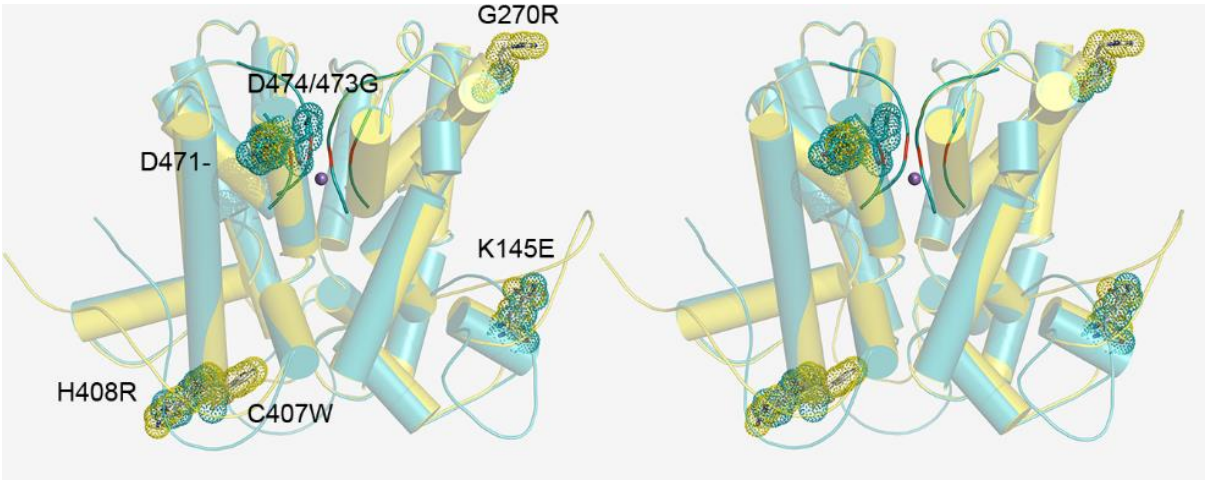

Fig. 4

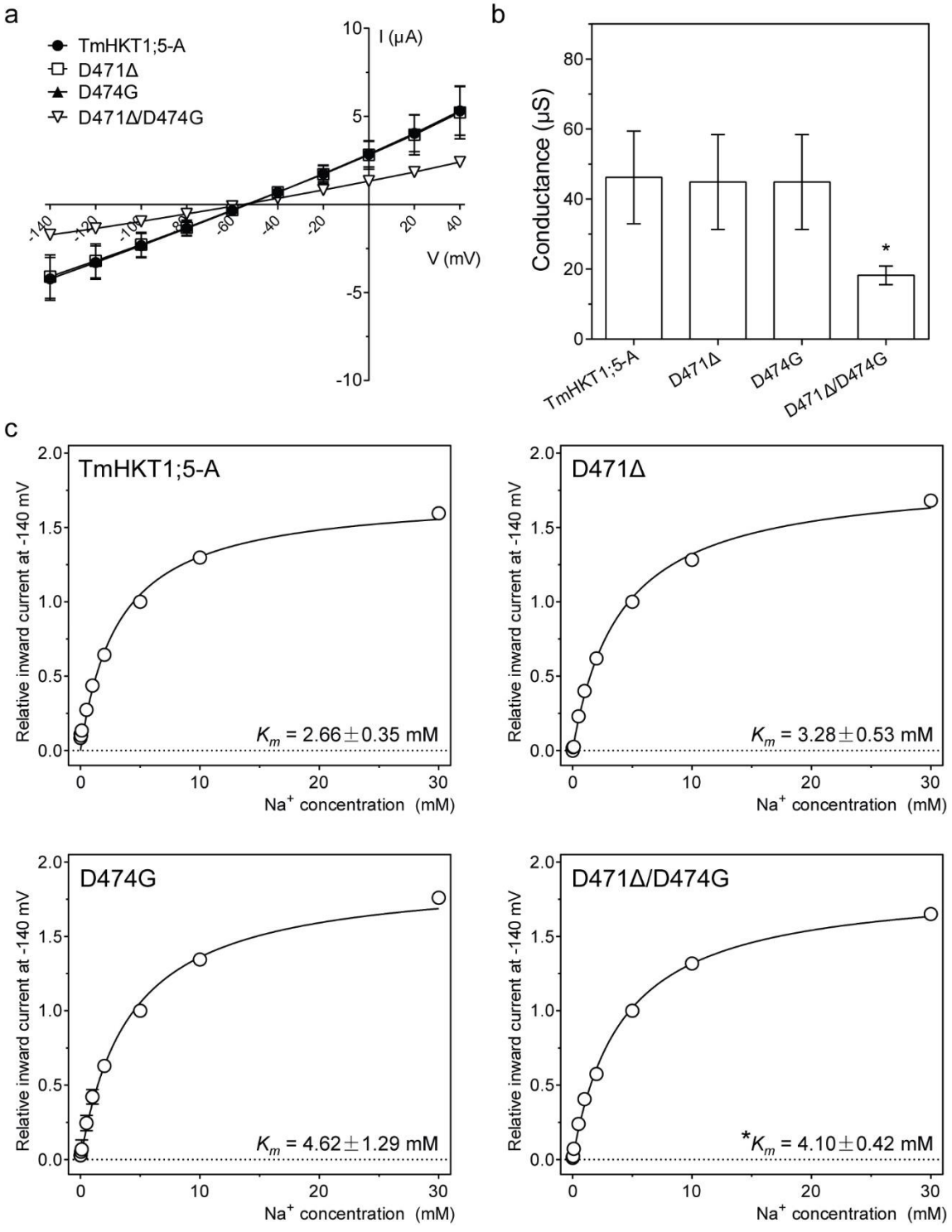
a
TmHKT1;5-A
D471Δ
D474G
D471Δ/D474G
I (μA)
V (mV)
b
Conductance (μS)
TmHKT1;5-A
D471Δ
D474G
D471Δ/D474G
c
TmHKT1;5-A
K_m = 2.66±0.35 mM
D471Δ
K_m = 3.28±0.53 mM
D474G
K_m = 4.62±1.29 mM
D471Δ/D474G
*K_m = 4.10±0.42 mM
Relative inward current at -140 mV
Na+ concentration (mM)

Fig. 5

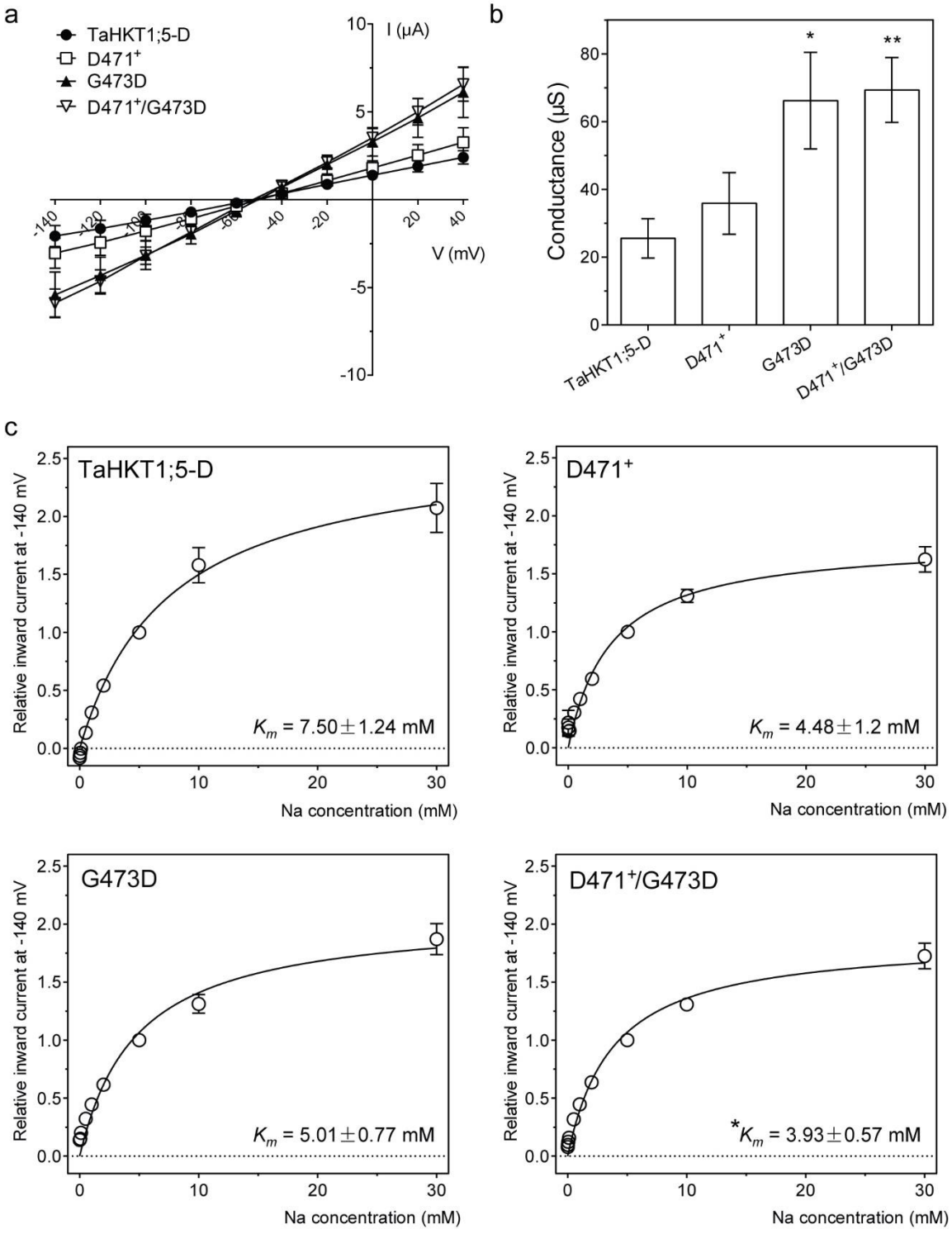
a
TaHKT1;5-D
D471+
G473D
D471+/G473D
I (μA)
V (mV)
b
Conductance (μS)
TaHKT1;5-D
D471+
G473D
D471+/G473D
c
TaHKT1;5-D
Km = 7.50±1.24 mM
D471+
Km = 4.48±1.2 mM
G473D
Km = 5.01±0.77 mM
D471+/G473D
*Km = 3.93±0.57 mM
Relative inward current at -140 mV
Na concentration (mM)

Table 1. A summary differences in amino acid residues between TmHKT1;5-A and TaHKT1;5-D that may significantly affect transport rates.

Residue number	Substitution		Predicted structural consequence of residue substitution or deletion
	TmHKT1;5-A	TaHKT1;5-D	
145	K	E	A change from a basic to an acidic residue. Likely to affect the local structure.
207	G	R	A substantial change in charge and volume of side chain. Expected to significantly alter the local structure.
407	C	W	Large difference in volume of a side chain at the base of an α-helix. Change in orientation of the α-helix.
408	H	R	Presence/ absence of the imidazole group from His. Significant change in the orientation of an α-helix, when combined with the C407W substitution.
471	D	-	Addition of an extra amino acid residue. Significant impact on a local structure.
474/473	D	G	Large charge difference combined with change of the volume of the side chain. Effect on packing of the structure, when combined with the nearby D471- substitution.